U.S. CONSUMER PRODUCT SAFETY COMMISSION
WASHINGTON, DC 20207

Todd A. Stevenson
Deputy Secretary and
Freedom of Information Officer
Office of the Secretary

Tel: 301-504-0785X1239
Fax: 301-504-0127
Email: tstevenson@cpsc.gov

January 5, 2001

03102CON
4/40

John F. Schilling
J.F. Shea Co., Inc.
655 Brea Canyon Road
Walnut, CA 91788-0489

Re: FOIA Request S0100115: Consolidated Industries Furnaces / Volmer-Gray Engineering Laboratories, Inc., "Investigation of Horizontal Forced-Air Furnaces Manufactured by Consolidated Industries, Inc., to Verify Furnace Failure and to Identify Failure Modes," May 2000

Dear Mr. Schilling:

Thank you for your Freedom of Information Act (FOIA) request seeking information from the U. S. Consumer Product Safety Commission (Commission). Enclosed are copies of the records responsive to your request: Volmer-Gray Engineering Laboratories, Inc., "Investigation of Horizontal Forced-Air Furnaces Manufactured by Consolidated Industries, Inc., to Verify Furnace Failure and to Identify Failure Modes," Contract CPSC-S-97-5316, Guthorn and Zaminski, May 2000.

Processing this request, performing the file searches and preparing the information, cost the Commission $60.00. In this instance, we have decided to waive all of the charges.

Sincerely,

Todd A. Stevenson

Enclosures

Failure Analysis

Accident Reconstruction

Safety Engineering

Fire Analysis

VOLLMER-GRAY

ENGINEERING LABORATORIES, INC.

MFR/PRVLBR NOTIFIED 1/22/01

- No Comments made
- Comments attached
- Excisions/Revisions
- Firm has not requested further notice

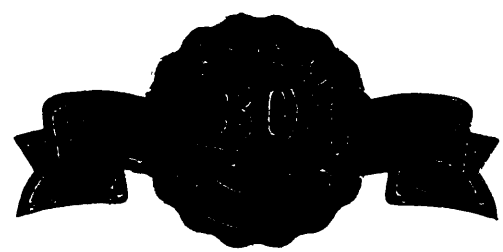

VOLLMER-GRAY
ENGINEERING LABORATORIES, INC.

Laboratory Number 970606

"An Investigation of Horizontal Forced-Air Furnaces Manufactured by Consolidated Industries, Inc., to Verify Furnace Failure and to Identify Failure Modes"

Prepared for:

U.S. Consumer Product Safety Commission
Office of Compliance
Room 613
Washington, D.C. 20207

Michael Gidding and Eric Singer
Project Officers

In fulfillment of
Contract No. CPSC-S-97-5316

May 18, 2000

1403 W. Gaylord St. Long Beach, CA 90813 Tel: 562-437-6468 Fax: 562-432-1805

TABLE OF CONTENTS

I. Objectives 1
II. Scope 1
III. Introduction 1
IV. Historical Information 3
V. Categorization 5
VI. Visual Examination 6
A. Burners 6
B. Heat Exchangers 10
VII. Field Operational Parameter Characterization 13
VIII. Furnace Background Characterization 15
IX. Metallurgical Analysis 16
A. Chemistry 16
B. Microstructural Evaluation 18
1. As-Manufactured 18
2. Aluminized Coating 19
3. Effect of Manufacturing Processes 20
4. In-Service Conditions 23
5. Oxide Thickness Measurements 23
6. Microstructural Effects 25
7. NOx Rod & Clip Microstructures 26
8. Burner Discoloration Evaluation 26
9. Heat Exchanger Microstructure 27
10. Microhardness 28
C. Metallography of Heat Exchangers 28
D. Scanning Electron Microscopy (SEM) 30
1. Burner Category 1 30
2. Burner Category 5_0 32
3. Burner Category 5 33
4. Burner Category 5+ 34
5. Burner Category 6 35
X. Summary 37
XI. Conclusions 41

OBJECTIVES

To perform a failure analysis of the Consolidated Industries burner and heat exchanger design.

SCOPE

The analysis tasks have been designed to yield information regarding specific performance characteristics of the 1983 through 1992 HAC and HCC horizontal forced air Consolidated furnaces with California emissions "NOx rods".

INTRODUCTION

Ninety-six furnaces were obtained from Costain Homes, Inc. The furnaces were removed from residences located in Chino, Murrieta, Temecula, Redlands, and Victorville, California. The units consisted of HAC/HCC models of size 60,000 BTUH (3 burner), 75,000 BTUH (3 burner), and 100,000 BTUH (4 burner). Prior to removal, field operational parameters were observed and measured by technicians of Westpac Air Conditioning, 601 South Milliken Avenue, Suite R, Ontario, California, under the supervision of Rod Trusler, Vice-President. This data included: model number, serial number, BTUH rating, limit switch settings, temperature rise in the as-found condition, external static pressure in the as-found condition, clock time for gas flow, gas valve pressure, temperature rise after installation of a new air filter, and external static pressure after installation of a new air filter.

The 96 furnaces were visually examined. All identification information originally placed on the units by the manufacturer or later added by the removal technicians (such as address of the home from which the unit came, etc.) was recorded. The furnaces were then disassembled. The disassembly involved removal of the burner and all lower panels so as to fully expose the bottom of the heat exchanger. Each furnace was examined visually and dimensionally, and documented photographically. The panels directly below the burner were examined for evidence of localized heating. The heat exchangers were examined for expansion joint cracking at the return and supply ends. They were also examined for any evidence of local heat discoloration, degree of oxidation, cracking, and rupture breakdown in the exchanger. The exchanger modules were numbered 1 through 6 (3-burner furnaces) or through 8 (4-burner furnaces). The exchanger length was 24". Each burner assembly was microscopically examined. The burners were examined for burner tube discoloration patterns, NOx rod discoloration and warpage, burner fold cracking and port opening, and other damage. The burner folds were numbered 1 through 31 beginning at the manifold end. NOx rod clips were located at folds 1, 8, 16, 24, and 31. As a reference, fold number 24 (with clip) corresponded approximately to an exchanger position 18" from the return end. The burner tubes were numbered either 1 through 6 (3-burner furnaces), or through 8 (4-burner furnaces) starting with the first viewed burner as number 1 with reference to a manifold to the right.

The burners and exchangers were categorized separately based on visual characteristics representing degree of use, state of degradation and progression of failure. The categorization parameters are indicated in Table 1. The field data was summarized and compared to the categorization findings. Representative units from each categorization were selected for further testing. Metallurgical samples were then removed from the selected units. Metallurgical

mounts were made from 85 samples: 38 heat exchanger and 47 burner samples (includes 8 "full" mounts defined as the NOx rod, clip and burner fold in relative position as found during usage). Scanning Electron Microscopy (SEM) samples totaled 32, which included 8 exchangers and 24 burner folds/ports. Energy Dispersive X-ray Spectroscopy (EDS) analysis was used on 8 burners and 8 exchangers. Bulk chemistry was performed on 30 samples: 10 burners, 9 exchangers, 7 rods, and 4 clips. Micro-hardness measurements were made on 48 samples: 19 exchangers, 21 burners, 4 rods, and 4 clips. The above data, readings, observations and characteristics were analyzed and summarized.

HISTORICAL INFORMATION[1]

Donald Hussong, Chief Engineer and Richard Weber, President, designed the Horizontal Forced Air Furnace model "HAC" in 1979 and began to sell it in 1983. This furnace had a completely new burner and exchanger design, not based on any pre-existing furnace. The material used for the burner tubes is T140 aluminized steel. The burner ports are made by a "progressive die method" where dies punch holes in the steel. The burner tube is formed by a single piece of steel which is folded and crimped to form the ports. This horizontal furnace could be mounted directly onto wood. The first NOx rod-equipped furnace for California was sold in 1984/5. The rods were simply added to the existing burner design with "no changes to the furnace . . . other than clips." The rods were made of 330 stainless steel. Prototype testing/evaluation notes of the NOx rod-equipped units tested between 1982 and 1984 revealed that the rods exhibited a hot spot

[1]The information in this section is based on deposition testimony and documents produced in private litigation, documents provided by Consolidated to CPSC, and personal experience and observations.

or region of higher temperature. In this hot spot region, the "rods glowed red." The non-NOx rod HAC design was fully tested by the American Gas Association (AGA) in the summer of 1983. The NOx rod unit was not fully tested, but rather given "abbreviated" testing due to the "relatively small change." The heat exchangers were originally made out of cold rolled steel. In 1987, Consolidated changed the exchanger material from 18 gauge cold rolled steel (CRS) to 18 gauge aluminized steel. The NOx rods were removed and replaced by screens in the early 90's.

The typical model numbers for Consolidated furnaces, HCC100NDSRX, display the following information. HCC stands for Horizontal, Model C and Cold rolled steel exchanger. (Models with aluminized steel heat exchangers used the designation "A" instead of "C".) The number 100 is the KBTUH rating. N is natural gas, DS is control type, R is for relay for blower, and X is for NOx rods.

Consolidated specified the furnaces' recommended maximum operating parameters as a temperature rise of 55°F, and an external static pressure of 0.50" water column. ANSI Standard Z21.47a-1983 states that the *MINIMUM* static pressure is to be 0.30". No maximum is given; that determination is thus up to the manufacturer. Consolidated selected the 0.50" value based on adding 0.30" (taken from the ANSI standard) to the change in flow which occurs when adding an air conditioning coil, resulting in 0.50" total. Consolidated then made this its *MAXIMUM* external static pressure. Consolidated has stated that the design input BTUH value, which is posted on the side of the furnace, is the "maximum allowable firing rate."

Furnace components have been evaluated in other cases. As part of the analysis in the *Salah vs. Consolidated* Class Action lawsuit, furnaces were examined from three housing projects, all in northern California. The elevations of the homes were all below 2000'. A significant

number of the furnaces were disassembled, allowing for the burners and heat exchangers to be examined. The criteria for categorizing the degree of degradation of the burners and heat exchangers are outlined in the next section of this report. The evaluation of the 51 burners examined revealed that 96% were at or beyond a category 5_0. The percentage of burners at or beyond category 6 was 45%. All of the non-NOx units were at a category 1 or 2. Approximately one-half of the exchangers were at or beyond a category 8_0. Field data was recorded prior to removal of the furnaces from a significant number of homes. In one housing project, 46 temperature rise data points were recorded. With reference to the Consolidated requirement of a maximum temperature rise of 55°F, 91% of the findings were proper. The recommended maximum external static pressure is 0.50". The percentage of units with a proper external static pressure was 49%. The final or ideal external static pressure averaged 0.51" water column, which is just slightly below the maximum allowed.

In the Woodbridge Cove lawsuit, 18 homes were field tested. The temperature rise was found to have been as per the manufacturer's specification in 89% of those tested. However, 100% of those tested had an improper external static pressure.

CATEGORIZATION

The burner and exchanger assemblies were examined and categorized. The categorization was somewhat qualitative for conditions 1 through 4 for the burners and exchangers in that surface appearance, coloration, degree of oxidation, etc., were the bases for the range of categorization. However, the remaining categories were based on specific physical characteristics such as cracking, displacement, etc. Category 5_0 for burners dealt with the embryonic stages of fold

degradation and cracking. Category 5+ was defined as the heaviest fold damage prior to sufficient degradation which allowed ports to begin to open up. Category 5 dealt with the large group of burners where the folds had substantial degradation and cracking but of a lesser degree than category 5+. Heat exchanger categorization from 1 through 4 dealt with increasing visual observance of macroscopic oxidation, discoloration, and thermal infliction. Exchanger category 8 was subdivided into five smaller divisions. Category 8 dealt with the range of findings from the first signs that localized heat damage was occurring (category 8_0), through the progression of further local thermal damage (categories 8_1 and 8_2), until the development of cracks in the local hot spot (category 8_3 through 8_4). Category 9 is self explanatory in that it required that the crack in the hot spot zone had grown to rupture with a crack opening displacement of larger than 1/8".

VISUAL EXAMINATION: BURNERS

The category 1 burner fold condition is shown in Figures A1 through A6. Visible are fold inner base corner cracks (A1, A4, A6), splits in the top shear burr (A2, A5), aluminized coating cracks (A1, A3), and cracks at the asymmetrical corner of the ports (A2, A5). A category 2 fold is shown in Figure A7, with oxidation appearing in the cracks on the top fold outer radial surface. The degree of oxidation increases for categories 3, Figure A8, and category 4, Figures A9 and A10.

In Category 5_0, cracks begin to form on the folds as shown in Figures A11 through A13. A progression of folds from 24 down through 18 are shown in Figures A14 and A15. Note the degree, pattern, and location of fold cracking. Category 5 folds are shown in Figures A16 through A18. The cracks are deeper, and with a higher concentration. A progression of category

5 folds from 27 down through 22 are shown in Figures A19 and A20. Note that the worst fold is 24, at the rod clip. Category 5^+ folds are shown in Figures A21 through A24. Figures A21 and A22 are of folds 28 through 24. Figures A23 and A24 are of individual category 5^+ folds.

Category 6 burner folds displayed heavy cracking. Figures A25 through A32 show folds 30 down through 19. Figure A25 shows folds 30 through27. Note that fold 30 is completely consumed, and 29 is partially consumed. Figure A26 shows folds 28 through 26. Figure A27 shows fold 27 which displayed a macroscopic crack propagating from the inner fold corner which progressed down to the base of the burner tube. Numerous smaller cracks of similar orientation exist. Figure A28 shows folds 27 through 24 (with rod clip). Figures A29 and A30 show folds 25 and 24, and 24 and 23 respectively. Note that the thermal degradation has inflicted the top areas of the ports. Figure A31 shows folds 23 through 21. Figure A32 shows folds 21 through 19. Figure A33 is an opposite viewpoint of the top area of two ports. Note the degree of cracking, discoloration, and the "veining" inside of the ports (lower arrow). Figures A34 through A38 are views of Category 6 folds. The degree of fold cracking is substantial. Note the displacement of the ports (opening mode) in Figure A34 (2 arrows).

Category 7 burner folds are shown in Figures A39 through A41. The folds shown are 27 through 23. The degree of local damage is massive. The folds are generally consumed, and the top areas of the ports are heavily cracked and distorted. The depth of thermal damage is substantially lower than the top of the ports. Figures A42 through A44 show folds 23 through 29. Figures A45 and A46 are of folds 28 through 23. Figure A47 is a top view of a failed burner in the latter stages of category 7.

Table 2 displays the percentage distribution of burner conditions for the 100,000 BTUH furnaces (both HAC and HCC) which were equipped with NOx rods. The majority (85.5%) had some degree of cracking, and thus were at or beyond category 5_0. Only 14.5% of the burners examined showed no signs of burner fold breakdown and cracking. 59.7% of all units exhibited degradation within the entire category 5 (5_0 through 5+). The single category with the most observances was 5 (29.0%). Burners which displayed the latter stages of breakdown (categories 6 and 7) were substantial (25.9%).

Table 3 shows the numerical distribution of folds which showed breakdown and cracking. Fold 24 (with NOx rod clip) was unanimously the first site where fold breakdown and cracking initiated, and the fold with the most occurrences of cracking. It is clear from Table 3 that the location of the zone of maximum fold degradation is at rows 4 and 5, centered about fold 24, and ranging from folds 20 through 28. Rows 3 and 6 had maximum damage about fold 24 with the zone of degradation ranging from folds 22 to 27.

Eight non-NOx rod units were examined and categorized by burner condition in the same fashion as noted prior. The eight consisted of six 100,000 BTUH units, one 75,000 BTUH unit, and one 60,000 BTUH unit. Table 4 shows that 100% of the burners in the 100,000 BTUH and 75,000 BTUH non-NOx rod units fell within categories 1 through 3. This means that the burners showed, at the most, "moderate discoloration", with no indications of any burner fold breakdown or cracking. This observation is in clear statistical contrast to the NOx rod equipped burners.

Table 5 shows the distribution of degradation categories for the smaller three burner tube units (50,000 and 60,000 BTUH NOx rod units). These units exhibited better results than the larger four-burner tube unit, in part due to the smaller width and enhanced cooling from the

surroundings. The two- and three-burner units have a decreased distance from the furnace centerline to the cooler-side faces of the burner compartment and thus operate cooler than the four-burner units. A clear majority (75%) were at or below a category 4, meaning no signs of fold breakdown or cracking. The remaining 25% fell into category 5 or 5+.

The majority of the burner assemblies (defined as over 50%) showed a strong discoloration zone on the panels underneath the burners indicative of high thermal infliction, with examples shown in Figures A48 through A50. These "hot spots" had a range of widths as shown in Table 6. The most common width was 8", with the average width being 6.6". The center points of the hot spots were predominantly located below burner folds 21 through 24, with the most being below fold 22, as shown in Table 7. The distribution of folds for burner rows 4 and 5 which were found to be above the lower panel hot spot is shown in Table 8. The bottom panels were physically located under folds 8 through 31. The majority (over 50%) of the discolored zones on the lower panels were found to run from fold 13 through fold 31.

The non-NOx rod burners examined showed that 86% of the 75,000 and 100,000 BTUH units had no lower panel hot spot type discoloration due to heat from the burner above. The one unit which displayed discoloration to the panel showed a pattern which started at fold 22, and was a maximum in width at fold 31 (the end of the panel). This pattern was of a different shape than that observed in the NOx units.

The sides of the NOx unit burner tubes displayed two macroscopically different patterns of heat-induced discoloration to the aluminized steel. One pattern was a deeper pattern in that the dark gray discolored regions covered most of the side of the tubes, as shown in Figure A51, whereas the second pattern was a shallow pattern that only discolored the top areas of the tubes.

Burners with similar categorizations were found that showed both types of patterns; it was even found that some burners exhibited both patterns adjacent to one another at rows 4 and 5. A majority of the burners (approximately 75%) showed the deep pattern. The longitudinal point where discoloration was the deepest, and thus the maximum, was below fold 25 on an average. The extent of the discoloration is shown in Table 9 which shows the numerical distribution of folds located above the darker gray zones. The majority of the discolored zones (over approximately 50%) were located below folds 20 to 30.

The NOx rods were found to display thermal-induced warpage and combustion residue buildup, as shown in Figures A52 and A53. The degrees of both conditions were at times massive. Table 10 shows the distribution of rods having varying degrees of warpage and/or residues. Over 50% of the rods showed at least some warpage, and 44% showed at least some residues. The rods which were found to be warped were predominantly the "inner" rods defined as those above the formed sides of the folds and toward the inside of each tube. These rods were labeled 2, 3, 6, 7, 10, 11, 14, and 15 of the 16 total rods. It was found that in 15% of the burner assemblies, all of the inner rods showed warpage and that 10% of the rods showed residue buildup. One burner assembly displayed massive consumption of all but three rods, as shown in Figures A54 through A58. The chemical analysis of these rods is discussed under the Chemistry section, and explains the rationale for the damages noted.

VISUAL EXAMINATION: HEAT EXCHANGERS

The location of burner fold 24, the first fold to crack, and the center point of all subsequent degradation and breakdown of the burner, was found to be below the 18" point of the

24" long heat exchanger. The maximum damage to the burners was also greatest along rows 4 and 5, which were directly below exchanger modules M3, M4, M5, and M6. The location of exchanger breakdown was centered at 18" and at 1" above the bottom nodule welds.

The examination of the heat exchangers revealed a range of conditions relative to the degradation and breakdown. A category 1 heat exchanger condition at the 18" horizontal and 1" vertical position is shown by unit 452 module 3 in Figure E1. The surface has relatively nil discoloration and oxidation. A category 2 exchanger is shown by unit 473 module 5 in Figures E2 and E3. A category 3 exchanger is shown by unit 490 module 5 in Figures E4 and E5. A category 4 exchanger is shown by unit 464 module 5 in Figures E6 and E7, and by unit 484 module 4 in Figures E8 through E10. A category 8_0 exchanger is shown by unit 470 module 5 in Figures E11 through E13, and by unit 476 module 3 in Figures E14 and E15. Note the coloration bands off of the weld, and centered around the 18" to 19" position. A category 8_1 exchanger is shown by unit 475 module 4 in Figures E16 through E18, and by unit 480 module 3 in Figures E19 through E21. A category 8_2 exchanger is shown by unit 421 module 3 in Figures E22 through E24, and by unit 479 module 6 in Figures E25 through E27. Note the surface oxidation and cracking in the oxide layer. A category 8_3 exchanger is shown by unit 421 module 6 in Figures E28 through E30, by unit 430 module 4 in Figures E31, and by unit 475 module 3 in Figures E32 through E35. A category 8_4 exchanger is shown by unit 430 module 6 in Figures E36 through E38. Note the localized discoloration, oxide buildup, oxide cracking and stages of bulging. A category 9 exchanger, with full rupture, is shown by unit 430 module M3 in Figures E39 through E45. The entire rupture was 3" long and was centered about the 18" mark, and 1" from the weld.

FIELD OPERATIONAL PARAMETER CHARACTERIZATION

Operational parameters were measured in the field prior to removal on approximately one-half of the 100K BTUH furnaces submitted for analysis. The recorded data included temperature rise and external static pressure in the as-found condition, temperature rise and external static pressure after installation of a new air filter (and opening of all vents, registers, etc.), gas valve pressure, and clock time for gas flow (reflective of relative firing rate). The field data along with the burner and heat exchanger categorization results are shown in Table 14. The as-found temperature rise data ranged from 20°F to 54°F with one data point at 72°F. The averages for the data are shown in Table 15. The average temperature rise was 34.14°F. The as-found external static pressure ranged from 0.44" to 0.96". The average was 0.66". The ideal temperature rise ranged from 20°F to 57°F with one value at 72°F. The average was 35.81°F. The ideal external static pressure ranged from 0.44" to 0.78". The average was 0.61". The gas valve pressure ranged from 2.8" to 3.25", with one data point at 3.9". The average was 3.05". The bulk of the firing rate time data ranged from 30 seconds to 37 seconds with three readings beyond of value 57, 58 and 75 seconds. The average of the data was 37.55 seconds. For a 100K BTUH furnace, 36 seconds of gas flow would correspond to the rated BTU output (assuming a gas factor of 1,000 BTU per cubic foot).

The burner categorization versus field parameters are shown in Tables 16 through 21. Statistical analysis was performed to determine if any correlation between burner categorization and field parameters existed. Correlation theory was used to determine if two variables were related by a linear curve. The computer generated best-fit linear curve, using the method of least squares, was determined and plotted. Statistical linear correlation was calculated to evaluate the "scatter"

in the data. The coefficient of correlation r^2 was used to analyze the significance of the scatter. Table 16 displays the data for burner category versus as found temperature rise and shows significant scatter. The calculated coefficient of correlation, r^2, was 0.0447. This value is very near zero, and thus it can be concluded that there is "almost no correlation between the two variables". Table 17, which has burner category versus as-found external static pressure, has an almost horizontal best-fit linear curve. The coefficient of correlation was 0.0079. This number is even closer to zero, and it can be concluded that the two variables are not related. Table 18 shows burner category versus ideal temperature rise. The best-fit linear curve had a small slope of 0.0409, which indicates that burner condition is independent of the ideal temperature rise. The correlation coefficient was 0.0519 and indicates that no correlation exists. Table 19 shows burner category versus ideal external static pressure. The best-fit curve is shown, and the coefficient of correlation was 0.0124. Again, there is no correlation between the two variables. Table 20 displays the data for burner category versus gas valve pressure. The best-fit linear curve has a negative slope and an insignificant coefficient of correlation. In general, the burner degradation decreases as the valve pressure increases (directly opposite to the claim made by the manufacturer). Table 21 exhibits the data for burner category versus firing rate time. The best-fit curve is shown and had a very small slope, and the coefficient of correlation was again a very small number (0.044). Thus, there was no correlation between the two variables.

The heat exchanger categorization versus field parameters is shown in Tables 22 through 27. Statistical analysis was utilized to evaluate the correlations. Table 22 shows exchanger category versus as found temperature rise. The best fit curve is shown. The correlation coefficient was 0.0478, and reflects almost no correlation between the two variables. Table 23 shows

exchanger category versus as-found external static pressure. The best-fit curve is shown and was with minimal slope, indicating an independency. The correlation coefficient was again very small indicating no relationship between the two variables. Table 24 shows exchanger category versus ideal temperature rise. The linear curve has a slight positive slope. The coefficient of correlation value was 0.0322, and indicates almost no correlation between the two parameters. Table 25 plots exchanger condition against ideal external static pressure. The best-fit curve had a correlation coefficient of almost zero (0.0418), and thus no correlation existed. Table 26 shows the relationship for exchanger condition versus gas valve pressure. The r^2 value was near zero and indicates almost no correlation between category and valve pressure. Table 27 shows the data for exchanger condition versus firing rate time. The best-fit linear curve is almost at zero slope, indicating an independency between the two parameters. The coefficient was very small and, therefore, there was no correlation between the two variables.

FURNACE BACKGROUND CHARACTERIZATION

Table 28 displays the city of origin (Chino, Temecula, Murrieta, Highland), date of manufacture, capacity and type of burner (NOx rod versus Non NOx rod), as well as the program identification number, and categorizations for each furnace. Table 29 exhibits the correlation between burner condition and heat exchanger condition. The general correlation was that the heat exchanger condition lagged behind the burner by an average of one category. The best-fit linear curve for the data is shown. The coefficient of correlation (r^2), which is a measure of how well the linear curve relates to the data, was 0.4258. A perfect correlation would have given a value of 1. Thus, there is a low degree of correlation between the two variables.

The burner category breakdown relative to city origin is shown in Table 30. For Chino, 90% of the furnaces were at or beyond a category 5_0, with the maximum of 35% at category 5. For Highland, 78% were beyond a category 5+, with the largest percentage of 33% at condition 6. For Murrieta, 73% were at or beyond category 5_0, with a maximum percentage of 33% at condition 5. For Temecula, 76% were at or below a condition 4, with a maximum distribution at condition 3 (38%).

The burner category versus year of manufacture is shown in Table 31. For 1987 manufactured furnaces, 71% of the burners were at or beyond a condition 5, with 64% at or beyond condition 5 plus. For 1988, 86% were at or below a condition 4. For 1989, only one furnace was noted, and it was at condition 4. For 1990, 89% were at or beyond condition 5_0, with 29% at or beyond category 6. For 1991, 78% were at or beyond a category 5_0, with the maximum percentage of 38% at condition 5.

The Temecula data and the 1988 data were noted to display behavior different from the rest. In reviewing the data, the following observations were noted. Seven of the 14 units were non NOx rod units with burner conditions mainly in categories 2 and 3. The remaining seven units were smaller capacity 60 KBTUH units equipped with NOx rods. Of these, 86% were at or below a category 4.

METALLURGICAL ANALYSIS

CHEMISTRY

Chemical analysis was performed on ten burner samples, nine heat exchanger samples, four NOx rod clip samples and seven NOx rod samples.

The ten burner samples consisted of: two from categories 1,4, 5_0 and 5, and one each from category 5+ and 6. Table 32 shows the chemical quantities of the 10 elements for the 10 samples. The findings were that all of the samples were of the same material defined as a low carbon steel (1005-1006). Note that the testing was performed on the base burner tube material with the aluminized coating removed.

The nine heat exchanger samples consisted of: two each from categories 1 and 4, and one from categories 8_0, 8_1, 8_2, 8_3, and 8_4. Table 33 shows the chemical quantities of the 10 elements for the nine samples. The conclusions again were that all of the exchangers were made of the same low carbon steel (1005-1006) material.

The four clip samples consisted of one from category 1, two from category 3, and one from category 5_0. The results are shown in Table 34. All four clips were made of 330 stainless steel.

The seven NOx rod samples consisted of one from category 1, two from category 3, one from category 5_0 and three from unit 472. The three samples from unit 472 were chosen because of massive consumption of many of the rods on that burner whereas rods on other furnaces were not consumed. The burner on unit 472 was categorized as a 3. Table C3 displays the chemical data. All of the rods were made of 330 stainless steel except for two of the consumed rods from unit 472 which were made of 302 stainless steel. The main differences chemically between 302 steel and 330 steel is that the 302 steel has 27% less nickel, which greatly reduces the high temperature exposure resistance.

MICROSTRUCTURAL EVALUATION

Burner Microstructure

As-Manufactured

Furnace burner sections that were categorized as Category 1 were used for evaluation of the as-manufactured condition. Samples in the L1, L2, T1, T2, and Full orientation were evaluated. Photographs of the burner samples are grouped by category. Category 1 samples are shown in Figures C1 through C37. Figures C38 through C43 show Category 2 samples. Figures C44 through C55 show Category 3 samples. Category 4 samples are shown in Figures C56 through C61. Category 5_0 samples are shown in Figures C62 through C86. Figure C87 shows a Category 5 sample. Figures C88 through C101 show Category 5+ samples.

Category 1 samples exhibited an equiaxed, relatively fine grained ferritic microstructure. Figure C20 shows a T2 orientation of burner 452 at 15x. As shown in Figure C27, grain size was a nominal ASTM grain size No. 10 based upon comparison with standard micrographs. The overall microstructure was consistent with a cold rolled and recrystallized low carbon steel sheet. At the fold, the microstructure had been disturbed, as shown in Figure C22. The fine grained ferrite is elongated with the greatest elongation occurring at the outer bend radius of the fold. The inner bend radius area exhibited folds and laps. Figure C25 provides a 200x view of the inner bend radius of burner 452. The micrograph shows the unetched inner bend radius. As can be seen, the bending and crimping operations created cracks extending into the base metal and damage to the coating. Figure C26 provides a higher magnification view of the inner bend radius. Longitudinal views of Category 1 samples are shown in Figures C3 through C9. Corner radius

cracks can be seen in Figures C4, C5, C6 and C9. Figures C7 and C8 show the extent of disturbed metal at the edge of the fold.

Aluminized Coating

The aluminized coating for the as-manufactured burner sections is shown in Figures C13, C14, C23, C24, C30, C31, C32, C33, C35, C36 and C37. In the least exposed samples, Category 1, two distinct layers could be observed. These layers appeared to be the relatively unchanged aluminum coating specified for this product. Figures C13 and C14 show the coating in a typical unformed area. The coating was identified as Type 1 aluminum coating. The Type 1 coating is comprised of an inner layer of aluminum-iron-silicon intermetallic on the steel surface and an aluminum-silicon alloy outer layer. Measurements of Category 1 layers produced a range of inner layer thicknesses from 0.12 to 0.16 mils and outer layer thicknesses of 0.14 to 0.76 mils. Average combined coating thickness was approximately 0.64 mils.

Coating thickness and condition varied around the fold on Category 1 samples. At the fold upper surface, the coating was cracked as a result of the folding operation. Damage to the aluminized coating was observed at the outer bend radius on the transverse (T1 and T2) sections. Figures C23 and C24 show the aluminized coating at 200x and 1000x. The inner layer had cracked and spalled resulting in a "gap-toothed" appearance. Figures C30 and C31 show a similar condition on a full section Category 1 sample. The coating thickness at the fold upper surface was approximately 0.14 mils inner, 0.44 mils outer, and 0.58 mils total. Along the fold leg, coating thickness was 0.16 mils inner, 0.56 mils outer, and 0.72 mils total.

Coating thickness variations were observed between the inner diameter surface and outer diameter surfaces of the legs coincident with the NOx rod clips. Coating remnants from the

outer diameter surface can be seen in the vicinity of the clip teeth. As a result of the contact with the clip teeth, the coating outer layer thickness was reduced. Figure C35 shows the inner leg at a distance of 0.16" from the top of the fold. Figures C36 and C37 provide closer views of the outer diameter and inner diameter surfaces, respectively. As can be seen, the inner diameter surface had an aluminized coating outer layer thickness that was about five times thicker than the outer diameter surface coating outer layer. It was observed that the clip teeth had entrapped remnants of the coating, as shown in Figure C34. This would indicate that, as the teeth engage the fold, the coating outer layer that it contacts is being sheared from the steel sheet, as shown in Figures C28 and C29. By comparison, those transverse samples without NOx rods had measured coating outer layer thicknesses of approximately 0.56 mils, whereas, the corresponding location with a clip installed had a coating outer layer thickness of 0.14 mil.

Effect of Manufacturing Processes

The T1 samples were selected to allow evaluation of the manufacturing processes on the edge condition of the folds. These samples were taken at the edge of the fold at the point where the fold legs intersect the port opening. Although all four of the T1 samples were from the same burner, 452, it was noted that the port opening wall heights varied from sample to sample. For instance, sample 452B had the port crimped wall intersecting the fold legs at a distance of approximately 0.06" from the top of the fold while the port straight wall intersected the fold legs at a distance of approximately 0.10" from the fold top. For purposes of comparison, scale measurements were taken from the Consolidated Industries burner assembly drawing. This showed the port crimped and straight wall heights as equidistant and approximately 0.057" from the top of the fold.

The average height of the straight and crimped legs for sample 452B was 0.08". This represents a 40% increase over the 0.057" nominal height depicted in the burner assembly drawing. The increase in height appears to be accomplished by stretching the fold legs during the bending and crimping operations. As the legs become stretched, localized yielding and fracture of the fold legs can occur.

Sample T1 452B sustained significant edge damage as a result of the creation of the fold, as shown in Figures C10, C11, C12, C15, C16 and C17. The crimped leg had a through-the-wall-thickness crack at the intersection with the port crimped wall. The crack was fairly shallow. Measurements from an L2 longitudinal sample showed cracking to a depth of 0.009" (see Figures C3, C4, C5, C6 and C9). Sample T1 452C total leg height was approximately 30% greater than the 0.057" nominal height. As shown in Figure C17, the crimped leg has yielded and partially cracked at the intersection with the port wall.

Bend radii were measured for a number of as-manufactured transverse samples. The bend radius is commonly expressed as the radius of a rod about which the sheet could be bent. The minimum bend radius is the radius of the smallest rod around which a sheet can be bent without cracking. Moderately severe forming can be achieved on aluminized steel sheet; however, requirements for corrosion resistance in service often limit the permissible severity of forming. Cracking and crazing of the coating may occur if the bend radius is too severe. This will reduce the service life of the sheet. Published data for corrosion resistant applications list a minimum bend radius of 0.5t (t = wall thickness) for sheet thicknesses of 0.0276" or less. For the 0.029" thick steel sheet used in the burners, the minimum bend radius would be approximately 0.015".

Figures C20 and C21 show sample T2 452. As can be seen, the bend is not uniform. Near the fold top, the bend radius was measured at approximately 0.0055". This is more than 2-1/2 times more severe than the recommended minimum bend radius. Sample T1 452C, shown in Figure C17 had a 0.0086" bend radius near the top of the fold. As was previously mentioned, the bend resulted in (1) cracking and spalling of the aluminized coating along the top of the fold, (2) folds and cracks of the steel sheet at the inner radius, (3) and yielding and cracking of the legs at the intersection with the port walls. Additional examples of malformed bend radii in Category 1 samples are shown in Figures C10, C28 and C29. Malformed radii were observed in higher degradation category samples, as illustrated in Figures C38, C47, C48, C62, C63, C72, C73, C80, C81, C82 and C87.

The bend radius appears to be the result of two distinct fabrication operations. The sheet is initially bent to a fairly large radius to produce the port opening. According to the burner assembly drawing, the port opening should be approximately 0.063". The corresponding bend radius of 0.0315" would be greater than the minimum radius listed and should provide adequate coating protection. The subsequent operation to crimp the inner leg and produce the fold has created the severe bend radii at the folds.

Corner radii between the port walls and the fold legs was measured. Radius values as low as approximately 0.004" were recorded. Edge cracks into the base metal were observed at several of the corner radii, as shown in Figures C3, C4, C5, C6 and C9. In general, the smaller the radius value, the greater the depth of cracking into the leg.

In-Service Conditions

Samples representative of the different degradation categories were selected from the burners. An evaluation of the extent of oxidation for the different categories was performed. A correlation was established between as-manufactured conditions and the level of deterioration of the burner folds.

Measurements were taken of transverse mounts (T2 and full cross-section) representing categories 1 through 5+. The fold leg thickness was measured at several locations. The results of thickness measurements are shown in Table 35. There was a progressive decrease in base metal thickness with an increase in degradation category. The greatest thickness decrease occurred within the range of 44 to 70 mils from the top of the fold on the fold inner leg (crimped leg). This corresponds with the fold leg intersection with the port crimped wall. As was previously noted, during fabrication this area can suffer extensive damage. Figures C41, C42, C49, C50, C69, C70 and C84 show the progression of oxide thickness increase and the reduction in leg thickness at this location. At Category 5+, the leg had completely separated, as shown in Figure C101.

Table 35 also illustrates the fold thickness at locations away from the fold inner leg. Decrease in leg thickness was minimal, as shown in Figures C43, C53, C54, C55, C71 and C79. Category 1 thickness measurements were 0.028" while Category 5 thickness measurements of 0.0268" were recorded at locations away from the fold inner leg.

Oxide Thickness Measurements

Oxide thickness measurements were made on samples representative of different degradation categories. On the longitudinal and transverse sections, oxidation was greatest at the top of the fold and at the fold inner leg near the top of the fold. Table 36 shows oxide layer

thickness for different categories. Figures C41 and C42 show the oxide layer at the fold leg near the top of the fold for a transverse Category 2 sample. Figures C39 and C40 show the top of the fold for the same sample. Figures C49, C50 and C51 show a Category 3 transverse sample. Figure C52 shows the fold top of a transverse Category 3 sample. Note the multiple oxide layers and the cracking between oxide and base metal.

Figures C56 through C61 show an increase in the extent of oxide thickness and cracking at the fold of a longitudinal Category 4 sample. Note the intergranular cracking into the base metal.

Figures C64 through C68 provide closer views of the oxide layer structure of a Category 5_0 sample previously shown in Figures C62, C63, C69 and C70. Additional transverse Category 5_0 sample oxide layer areas are shown in Figures C74, C75, C83, C85 and C86. Figures C74, C75 and C83 are at the top of the fold. Figures C85 and C86 depict the oxide layer at the side of the fold.

Beyond Category 1, an additional, third oxide layer was observed between the base metal and the inner aluminized coating layer. In the heavily oxidized areas, the coating inner layer thickness increased nearly one order of magnitude; a Category 5 sample measured 1.09 mils for the inner layer while a Category 1 sample measured 0.16 mils. Coating outer layer thickness typically doubled; 1.58 mils for the coating outer layer of a Category 5 sample compared to 0.72 mils for a Category 1 sample. However, the inner oxide layer thickness for this same Category 5 sample measured 12.57 mils. Increases in the coating layer thicknesses were attributed to oxidation within, and cracking of, the coating. In areas of the legs other than the top of the fold and the port wall

intersection, the extent of oxidation was minimal. Table 37 shows the change in oxide layer thickness as a function of category.

The oxide layers were characterized by a network of cracks. Cracks were through the oxide layer thickness, between oxide layers and between the oxide and the base metal. Figures C92 through C98 provide examples of the oxide layers and crack network. At the early stages of attack, oxidation of the base metal occurs predominantly via the network of transverse cracks in the aluminized coating. As might be expected, the areas where the coating has been most heavily damaged during fabrication show the earliest signs of oxidation and were the most heavily attacked.

Microstructural Effects

The as-manufactured burner aluminized steel sheet was characterized by an equiaxed, fine grained ferritic microstructure, as shown in Figures C2, C18, C19, C22, C23 and C26. Grain size changes were observed for burner samples from the other categories. Grain size increases were observed for each category. Category 2 T2 samples exhibited an ASTM grain size of 4 to 5 for most of the fold. The inner and outer edges had a distribution of ASTM grain sizes 8 to 9. Category 3 samples exhibited grain growth at the fold and down the legs, as shown in Figure C50. Grain sizes and distribution at the fold were similar to the Category 2 samples. Further down the leg, a transition from the as-manufactured ASTM grain size 10 was observed As shown in Figures C53, C54, and C55, there were a series of angled bands of large sized grains interspersed within the finer grained areas. As shown in Figure C59, Category 4 samples revealed grain size variations similar to those of Categories 2 and 3. Category 5_0 exhibited a range of grain sizes, as shown in Figures C68, C70, C71, C75, C77, C78 and C79. ASTM grain size ranging from 3 to 9 were observed at the upper end of the fold. Further from the top of the fold, ASTM grain size 9 predominates.

Category 5+ exhibited grain sizes 2 to 4 at the upper end of the fold and along the crimped leg. On the straight leg, the larger grains predominated down to the port wall intersection. Below that, the fine grain size (ASTM 9) predominated.

Category 4 and 5 samples exhibited intergranular (IG) cracking and heavily decorated grain boundaries in the vicinity of the leg/port wall intersection. Figures C56, C57, C60, C61, C76, C77 and C78 show the location and extent of cracking. In the most heavily deteriorated samples, grain boundary sliding, indicative of creep failure, was observed, as shown in Figures C88, C80, C90, C91, C99 and C100.

NOx Rod & Clip Microstructures

Typical NOx rod clip microstructures for a Category 1 sample are shown in Figures C102 through C105. Figure C102 shows the rod microstructure, while Figures C103 through C105 show various locations on the clip. The microstructure was typical of cold worked 330 stainless steel. Figures C102 and C103 depict a slightly sensitized condition as evidenced by a non-continuous grain boundary carbide network. Figures C106 and C110 depict a Category 2 NOx rod and clip. Figures C111 through C115 show a Category 5_0 rod and clip. There did not appear to be a significant change in rod and clip microstructural condition between the different categories.

Burner Discoloration Evaluation

Samples from burner 432 rows 4 and 5 were examined microstructurally. The samples were chosen because they exhibited different levels of discoloration. Row 4 exhibited discoloration to just below the NOx rod clip, whereas row 5 exhibited discoloration of nearly the full burner height. Both samples were observed at Fold 24. Control samples from Fold 1 of each row were also examined. Neither Fold 1 sample exhibited any discoloration.

The Fold 1 samples are shown in Figures C116 through C121. Both Row 4 and Row 5 Fold 1 samples exhibited fine equiaxed grain structures. Microstructure and coating conditions were similar to those previously observed on Category 1 samples. Row 4, Fold 24 is shown in Figures C122, C123 and C124. There was localized grain growth at the top of the burner inner wall and isolated grain growth along the upper length of the wall. Oxidation of the coating was observed over the length of the discolored portion of the burner. Figures C125 through C128 show the Row 5, Fold 24 area of the burner. The extent of grain growth and oxidation is much greater than for Row 4. Figures C127 and C128 illustrate the oxidation and deterioration of the aluminized coating. This process gives rise to the observed discoloration pattern on the burner.

Heat Exchanger Microstructure

Category 1 heat exchanger sections were examined to evaluate the as-manufactured condition. Figures C129 through C132 show longitudinal samples. Figures C133 through C137 show transverse samples. It was interesting to note that the weld along the base of the heat exchanger varied considerably from exchanger to exchanger, as shown in Figures C129, C132, C138, C139, C140 and C149. Variations were observed in the location of the weld, size of the weld, depth of weld penetration, and gap between heat exchanger walls.

The microstructure of the as-manufactured heat exchangers was similar to that of the burners. Grain size for Category 1 samples, as shown in Figures C130 through C135 varied between ASTM grain size No. 7 and No. 8. Grain growth was observed in the highest category samples. Category 4 samples still exhibited an ASTM grain size 7 and 8, as shown in Figure C145. Category 8_0 grain size increased to ASTM grain size No. 6 and No. 7, as shown in Figure C148. Categories 8_3 and 8_4 exhibited grain size No. 5 and No. 6, as shown in Figures C159, C162, and C166.

Oxidation and oxide layer thickness increased with the higher category samples. The oxide layer was fairly uniform in thickness and was characterized by an extensive network of lateral and transverse cracks. The progression of oxide layer thickness increase is shown in Figures C129 through C170.

Microhardness

Microhardness tests were performed on selected burners in the fold area, burner NOx rods, burner NOx rod clips, and heat exchangers. All tests were performed using a 100 gram load. Results are shown in Tables 38 through 41.

The burner fold areas exhibited a sharp drop in hardness for all categories beyond Category 1. The decrease in hardness is consistent with loss of cold-rolling strain hardening and with grain growth.

The burner clips and rods did not exhibit any significant hardness change between Category 1 and Category 5+.

Hardness values for the heat exchanger samples did not exhibit a significant change with increasing category.

METALLOGRAPHY OF HEAT EXCHANGERS

Thirty-eight exchanger samples were removed, mounted, polished and etched. Nineteen longitudinal and nineteen transverse mounts were prepared. The orientations were defined as longitudinal being parallel to the module welds, and transverse being perpendicular to the module weld. In each orientation there were the following samples taken from the 18" length and 1" height zone: two Category 1 mounts, one Category 2 and 3, two Category 4, 8_0, 8_1, and 8_2, three Category

8_3, one Category 8_4, and one Category 9. In addition, there were two mounts made from samples taken from a 6" length and 1" height zone (i.e., significantly away from the hot spot zone) of a Category 8_0, and Category 8_4 exchanger for comparison purposes.

A Category 1 sample from unit 452 module 3 is shown in Figure M1. The right half displays an "L" and refers to a longitudinal orientation of the cut running along the left side of the right half which became the mounted face. The left half displays a "T" at the top with a line running from right to left below the "T". The "T" refers to the transverse orientation, and the line below the "T" was later cut and made the mounted face. The "S" to the bottom of the lefthand samples corresponds to the portion of the sample utilized for SEM analysis. Some mount samples do not have the "S", which indicates that they were not used for SEM analysis. A second Category 1 sample from unit 431 module 5 is shown in Figure M2. A Category 2 sample is shown by unit 473 module 5 in Figure M3. A Category 3 sample is shown by unit 490 module 5 as in Figure M4. A Category 4 sample is shown by unit 464 module 5 as shown in Figure M5, and by unit 484 module 4 in Figure M6. A Category 8_0 sample is shown by unit 470 module 5 in Figure M7, and by unit 476 module 3 in Figure M8. A Category 8_1 sample is shown by unit 475 module 4 in Figure M9, and by unit 480 module 3 in Figure M10. A Category 8_2 sample is shown by unit 421 module 3 in Figure M11, and by unit 479 module 6 in Figure M12. A Category 8_3 sample is shown by unit 430 module 4 in Figures M13 and M14, and by unit 475 module 3 in Figure M15. A Category 8_4 sample is shown by unit 430 module 6 in Figures M16 through M18. A Category 9 sample is shown by unit 430 module 3 in Figures M19 and M20. The interior side of the hot spot degradation zone is shown in Figures M21 and M22. Note the degree of oxidation and cracking. A side view of the longitudinal face shows the amount of material consumption from oxidation, as shown in Figure

M23. The two samples taken from the 6" length and 1" height are a Category 8_0 from unit 476 module 3, as shown in Figures M24 and M25, and a Category 8_4 from unit 430 module 6, as shown in Figures M26 and M27. Note that the categorization of these two samples was based on the findings at the 18" and 1" zone, and not from the 6" and 1" area.

SCANNING ELECTRON MICROSCOPY (SEM)

The SEM analysis was in part utilized to confirm and to expand the observations made from standard laboratory binocular light microscopy relevant to the manufacturing of the burner assembly as well as to the failure process.

BURNER CATEGORY ONE

Thirty-two SEM photographs were taken of eleven Category 1 burner folds (defined as "new"). All were taken from unit 452 (non-NOx unit). The folds displayed a number of significant manufacturing flaws which developed from the die stamping and fold forming operations. The corners of the stamped port opening were sharp. A shear burr was formed to one side of the stamped edges. Upon forming the burner tube, and as the folds were made, the sharp corners and shear burrs were found to be prone to cracking. The asymmetrical forming of the ports on the inner side caused cracking to form at the corner between the angled face leading to the port and the longitudinal face on the inboard side of the port. The forming radius of the folds were below the minimum allowed for the aluminized steel sheet, and thus it was found that the aluminum coat was cracked on the outer rounded surface of the folds. The aluminum was predominantly missing, as expected, from the stamped edges.

Figure B1 of row 3 fold 15 displays cracking at several locations. There were several cracks along the side curved face of the fold (arrows 1 and 2), with Figure B2 showing the cracks at 80x. These cracks were due to splitting of the shear burr upon forming of the port. Cracks were also found at the inner base of the fold on the asymmetrically formed side (arrow 3), and at the corner of the port between the angled side and the inner longitudinal side (arrow 4). Figure B3 of row 3 fold 16 shows cracking along the fold shear burr (arrow 1), and at the inner base corner of the fold (arrow 2). Figure B4 shows a near top view of row 3 fold 17. Figure B5 is a close-up of the area noted by arrow in Figure B4. Note the two cracks which occurred due to the forming of the port and which were both from splitting of the shear burr. Figure B6 is a near frontal view of row 3 fold 17. Figure B7 is an aft inner angled view of the same fold. Note the shear burr and splitting/cracks (arrows 1 and 2), and aluminum coating cracks (arrow 3). Figure B8 is an aft view of row 3 fold 17 and shows the top fold shear burr cracks, and the inner base corner crack (arrow). Figures B9 and B10 show row 3 fold 17 from the front side, and exhibit cracking nearly identical to that found on the aft side (Figure B8). Note that the faces of the sheared surfaces have very significant, parallel tool markings, as shown by arrow 1 in Figure B10. Figure B11 is a close-up of the inner corner base crack for row 3 fold 17 shown by arrow 1 in Figure B9. Figure B12 is a close-up of the top shear burr crack shown by arrow 2 in Figure B10.

Figure B13 shows row 3 fold 25 from a front direction. Note the sharp corner on the outer side (arrow). Figure B14 is a close-up of the top fold shear surface and burr crack. Figure B15 is a frontal view of row 3 fold 26, which displays similar cracking, and shear surface characteristics. Figure B16 shows the top surface of the fold. Note the aluminized coating cracks. Figures B17 and B18 are higher magnification of the coating cracks. The cracking is oriented 90° to the direction

of fold forming. Figures B19 and B20 show row 3 fold 27 from an aft direction. Note the cracking along the fold burr, inner base corner (arrow 1), along the asymmetrically formed area of the port (arrows 2 and 3), and the sharp outer base corner. As can be seen, the quality of the stamped faces differs from fold to fold, on even the same burner row. Figure B21 shows the front side of row 3 fold 28.

Figure B22 is an aft view of row 4 fold 25. Figure B23 displays an aft view of the shear burr area on the front side of row 4 fold 25. Note the splitting/cracking in the burr (arrows), and cracking in the coating. Figures B24 and B25 are similarly oriented views of row 4 fold 26. Figure B26 is an aft view of row 4 fold 27. The inner base corner crack is shown at 50x in Figure B27.

BURNER CATEGORY 5_0

Fifteen SEM photographs were taken of eleven Category 5_0 folds. Figure B28 displays an aft view of unit 478 row 4 fold 23. Note the degree of oxidation which covers the original sheared surfaces, and the deeper crack in the top curved edge of the fold (arrow). Figure B29 is a top view of the same fold, and exhibits longitudinal and transverse cracking and oxidation on the top fold area. Figures B30 and B31 are views of each end of unit 478 row 4 fold 24. The NOx rod clip can be seen in both figures. Both views show major cracking across the top of the fold, and at the inner base corners of the fold (arrows). Figures B32 and B33 show both ends of unit 478 row 4 fold 25. Note that there is less cracking of the top surface, but some inner base corner cracking. Figure B34 is a higher magnification view of the top crack in Figure B32 (arrow). Note that this cracking, though of lesser extent, is similar to that shown in Figures B30 and B31. The

sequence from fold 23 through 25 on a typical Category 5_0 was such that a maximum cracking and oxidation occurs on fold 24, with less at 23 and 25. Folds 22 and 26 were usually found to have less cracking than folds 23 and 25.

Figures B35 through B37 show unit 425 row 4 folds 23 through 25 from the aft side. Cracks have developed predominantly from the splits in the fold top shear burr and from the inner base corner. Severe oxidation has consumed numerous original surface features. Figures B38 and B39 are of unit 425 row 5 folds 23 and 24 from the front side. Again, cracking has extended from the manufacturing-induced cracks. Oxidation development on the curved top surface of fold 23 is visible in Figure B38 (arrow). Figure B40 is an inner side view of fold 24. Note the inner base corner cracking on both the front and the aft sides and along the top fold surfaces. This is a strong example that cracking from the inner base corner is propagating from the manufacturing-induced cracks. Oxidation development is apparent. Figure B41 is of fold 25, and displays the top fold surface oxidation (arrow 1) and the cracking leading off of the top fold shear burr (arrows 2 and 3). Figure B42 shows unit 427 row 5 fold 24 and the degree of cracking and oxidation common for fold 24 on a row 4 or row 5 burner tube in the Category 5_0 condition.

BURNER CATEGORY 5

Twenty-nine SEM photographs were taken of six Category 5 folds. Unit 473 row 5 folds 23 through 25 were examined. Figure B43 is a top view of unit 473 row 5 fold 23. Cracking exists off each top end of the fold from splitting/cracking in the shear burrs, with the right end shown in Figure B44. Oxidation is developing across the top of the fold. The tops of the adjacent port walls show cracking (arrow), as shown in Figure B45. The front side of fold 23 is shown in

Figure B46. The degree of cracking and oxidation is visible. Fold 24 of unit 473 row 5 is shown in Figure B47, with higher magnification views shown in Figures B48 and B49. Note the loss of oxidized material and depth and extent of cracking. The inner base of the fold is approaching full separation. Figure B50 is an aft view of fold 24. Figure B51 is an inner aft view of fold 24 and shows the amount of material loss from the end of the fold. Figure B52 is an inner front view of fold 24. Figure B53 is a frontal view of fold 24 prior to NOx rod clip removal. Figure B54 shows the top of the port walls adjacent to fold 24 toward fold 25. Note the cracking along the wall. Figure B55 is a top view of fold 25 on unit 473 row 5. Note that the degree of damage is less than on fold 24. However, there is substantial loss of oxidized material from the top of the fold. Figure B56 is an aft view of fold 25 which has lost much of the fold edge. Figure B57 and B58 shows the front side of fold 25 and the loss of material from the oxidized surface layer.

Unit 466 row 5 folds 23 through 25 were examined. Figures B59 and B60 show the loss of top surface oxidized material from fold 23. Figures B61 and B62 show an inner top and inner side view of fold 24. The fold has substantial loss of top surface oxidized material, and nearly complete separation of the fold from the inner wall of the port. Figure B63 is an aft view of the fold. Figures B64 and B65 are angled views from the top inner area. Figures B66 through B68 show fold 25. Again, the damage is less than fold 24, but shows that substantial top surface oxidized material has been lost and substantial cracking has occurred.

BURNER CATEGORY 5+

Twelve SEM photographs were taken of ten folds from row 4 of unit 489. Folds 17 through 22, and folds 26 through 30 were examined to show the extent of damage outside of the fold

region 23 through 25. Figures B69 through B74 show folds 17 through 22. Note that fold 17 and 18 have moderate amounts of oxidation but are relatively without cracking. Fold 19 begins to show cracking and heavier oxidation, as shown in Figure B71. Folds 20 through 22 display significant loss of oxidized surface material. Note the oxide "veins" leading down from below the inner side of the folds. These are regions where the aluminum coating cracked and the underlying iron-based material oxidized profusely on a local level. Figure B75 shows the veins at 50x. Folds 26 and 27 show similar but heavier damage in that there is full separation of the fold, as shown in Figures B76 and B77. Folds 28 and 29 suffered loss of oxidized surface material, as shown in Figures B78 and B79. Fold 30, shown in Figure B80, was found to be similar to fold 17.

BURNER CATEGORY 6

Nineteen SEM photographs were taken of folds 18 through 31 on row 5 of unit 428. Figures B81 through B85 show folds 18 through 22. Note that all five folds are fully separated, heavily cracked and oxidized, with oxide veins, and with vertical cracking leading down from the base of the fold, as best shown on fold 21 in Figure B84 (arrow). Figures B86 and B87 show folds 23 and 24. Fold 23 is very similar to fold 22. Fold 24 has no remains of the fold. Figure B88 is a top view of fold 24. Figures B89 and B90 are similar views of fold 25. Figures B91 through B96 show folds 26 through 31. The degree of damage lessens as the folds progress toward fold 31. However, fold 31 still has full separation of the fold. Figure B97 is a higher magnification view of the oxide veins on fold 26 (arrow in Figure B91).

The SEM examination showed that the failure process involved locally massive oxidation of the folds. The failure involves: 1) oxide development which preferentially and

prematurely occurs at the surfaces without aluminum (stamped surfaces) and at the initial manufacturing-induced flaws and cracks which exposed base metal; 2) cracking of the oxide and base metal; 3) spalling of the oxide; and 4) further oxide buildup, followed by further cycles of cracking, and spalling.

Scanning Electron Microscopy (SEM) was utilized to examine eight heat exchanger samples from seven different categories. The samples were removed from the "hot spot" zone of modules M3, M4, M5 or M6. The samples were approximately 3" long and 2" tall, and were all centered at 18" from the return end and 1" up from the bottom weld. Two Category 1 rated samples were examined which came from units 431 module 5, and 452 module 3. SEM analysis of the surfaces showed a tight oxide layer without cracking or spalling, with typical findings as shown in Figure S1 from unit 431 module 5. The Category 8_0 sample taken from unit 470 module 5 displayed a similar appearance at 100X, as shown in Figure S2; however, there were sites of local oxide loss. The Category 8_1 sample from unit 480 module 3 showed a much more disturbed surface with thicker oxide growth, a more uneven oxide surface, and larger zones of oxide loss, as shown in Figure S3. The surface condition from a Category 8_2 taken from unit 421 module 3 is shown in Figures S4 through S7. The surface now begins to show cracks and early stages of spalling in the oxide layer. Examination of unit 430 module 4, which was categorized as an 8_3, revealed significant cracking defined by depth and length, as shown in Figures S8 and S10. The large cracks are surrounded by a matrix of smaller cracks. Other zones of cracking and local spalling are shown in Figures S11 and S12. The SEM examination included the fracture faces. An attempt was made to ascertain whether thermal fatigue cracking was involved in the failure process. Figures S13 through S15 are from a fracture face from unit 430 module 4. The arrow in Figures S13 shows the location of Figure S14,

and the arrow in Figure 14 depicts the location at which Figure S15 was taken. Figure S15 displays an oxidized fracture face which had semicircular/wavy markings which could be indicative of time-dependent crack growth. The observations were not conclusive as to whether fatigue cracking caused the observed markings. The Category 8_4 surface appearance from unit 430 module 6 was heavily cracked with areas of recent spalling of the surface oxide layers, as shown in Figures S16 through S19. The Category 9 zone from unit 430 module 3 involved a full rupture, massive secondary cracking, outward bulging type displacement, and loss of oxide material. The areas at and adjacent to the rupture are shown in Figures S20 through S25. The face of one of the fractures was examined. The sample chosen was a small secondary crack which was manually broken open so as to reveal the crack faces. The mechanically-induced overload zone displayed dimple rupture fracture. The surfaces immediately adjacent had an appearance as noted above, with an oxidized fracture face, as shown in Figures S26 through S28.

The Energy Dispersive X-ray Spectroscopy (EDS) analysis did not provide any information in addition to what has been summarized above.

SUMMARY

Ninety-six Consolidated furnaces were metallurgically examined. The burner degradation occurred at an advanced rate relative to the degradation of the exchanger. The first sign/step of the failure process for the burner is fold cracking. The majority (85.5%) of the 100,000 BTUH burners with NOx rods had at least some degree of burner fold cracking. One quarter (25.9%) of the burners were in the final stages of full failure. For the non-NOx rod units, 100% of the burners had no cracking. This is in clear statistical contrast to the NOx rod equipped units. Fold

24 along burner rows 4 and 5 were the first folds to crack, and the folds with the highest occurrence of cracking. The zone of maximum fold degradation ranged from folds 20 through 28 along rows 3 through 6. Over 50% of the burner assemblies had a visible "hot spot" discoloration zone on the panel below the burner. This hot spot averaged 6.6" wide, and ranged from folds 13 to 31. The sides of the burner tubes showed a dark gray discoloration zone which had a maximum depth down to the bottom of the tube at fold 25, and with a length from folds 20 to 30. The darkening of the aluminized steel was due to temperatures exceeding 950°F wherein the two-layer coating is developing into a single layer of AL-Si-Fe intermetallic. Over 50% of the NOx rods displayed warpage and 44% displayed residues from combustion. Several rods were found to have sustained massive consumption. Later chemical analysis showed that the consumed rods were made from 302 stainless steel, a lower grade of stainless steel than 330 grade. 302 grade stainless steel has 27% less nickel than 330 stainless steel. This reduced nickel content greatly decreases high- temperature resistance.

Fold 24 of the burner corresponded to a point 18" along the 24" exchanger. The exchangers displayed a local hot spot where metallurgical breakdown occurs. The hot spot was centered at 18" along the exchanger, 1" above the bottom weld, and at the four central module halves. The hot spots were noted in 14.7% of the exchangers. Five of the exchangers exhibited more than one hot spot, with one even having three such zones. The typical exchanger had cracking on the supply and/or return expansion joints. The average transverse cracks on the expansion joints were 7.1" long on the supply side and 9.2" on the return side. The average longitudinal crack length was 0.9" for the supply end and 1.0" for the return end.

Field operational parameters were measured. The temperature rise averaged 34.1°F in the as-found condition, and 35.8°F in the ideal condition. The Consolidated manual gives a maximum of 55°F. The external static pressure was measured to be an average of 0.66" in the as-found condition, and 0.61" in the ideal condition. The Consolidated manual specifies a maximum of 0.50". The manifold gas valve pressure averaged 3.05". The average firing rate time was 37.55 seconds. Utilizing the method of least squares and statistical linear correlation showed that there was no correlation between the degree of burner or exchanger breakdown and any of the field operational parameters. The data in most cases resembled "scatter".

Chemical analysis identified the materials utilized for the various components. The burner base material, underneath the aluminized coating, and the cold rolled steel (CRS) exchanger were both made of 1005-1006 low carbon steel. The NOx rods and clips were made of 330 stainless steel, except for a few rods noted above which were made of 302 stainless steel.

Metallographic analysis of the as-manufactured material conditions showed the following. The burner tube material had an equiaxed, ferritic structure, with a fine No. 10 grain size, consistent with a cold rolled and recrystallized low carbon steel sheet. The aluminized type 1 coating had two distinct layers. The thickness of the inner layer ranged from 0.0012" to 0.0016". The outer layer ranged from .0014" to .0076". The average coating thickness was .0064". The folds showed grain elongation in the base metal at the outer bend radius of the fold. The inner bend radius had heavy damage, with folds, laps, and cracks due to the folding and crimping fabrication steps. The burner folds in the as-manufactured condition revealed different heights of the two port walls due to stretching during the bending and crimping operations. This deformation caused localized yielding and cracking which was concentrated at the top of the crimp, which is at the base of the

fold. The fold bend radii were below the minimum allowable value by a substantial amount. The minimum radius should have been 0.015". The actual values averaged 0.0055", with some radii as low as .0030". The result of the extreme fold bend radii was cracking and spalling of the aluminized coating along the outer radius of the fold and heavy microstructural damage and cracking at the inner radius of the fold. The crimping of the fold formation was responsible for the radius dimensions and resulting damage. The lower inner fold base corners, adjacent to the port, had very sharp corner radii (as low as 0.004") and exhibited cracking on most of the folds examined.

Microstructural examinations of the service-degraded assemblies revealed the following. There was a progressive decrease in base metal thickness with increase in degradation category. The location of maximum metal thickness loss was at the top of the inner fold leg (crimped leg). Oxide thickness was a maximum at the top of the fold, and at the top of the inner fold leg (crimped leg). The oxide developed between the aluminized coating and the base metal due to the manufacturing-induced damage to the coating. The oxide layers were characterized by a network of cracks. Grain growth, intergranular cracking, and heavily decorated grain boundaries were noted. In the most heavily deteriorated samples, grain boundary sliding was observed indicative of creep failure.

SEM analysis provided the following observations of the results of the die stamping and fold forming operations. The corners of the stamped port openings were very sharp. Most folds showed cracks at the lower inner fold corner (crimp leg). The shear burr splits/cracks as the fold is formed. The aluminum coating was predominantly missing from the sheared edges. The quality of the sheared surfaces varied significantly, even from fold to fold on the same burner. The aluminized coating was cracked along most of the outer radius surface of the folds.

SEM analysis showed that the initial cracking due to service induced degradation occurred across i) the top of the fold, propagating from the splits in the shear burr and ii) across the lower inner fold propagating from the lower base corner cracks, which were induced by the crimping operation during manufacturing. The overall fold outer surface was degraded by oxidation. As the breakdown of the fold progresses, the top of the fold begins to lose substantial portions of material due to oxidation, cracking, and spalling of the oxide from thermal cycling and further oxidation. By Category 5, folds in the heaviest damaged burner zones start to become fully fractured due to the oxidation-induced process noted above. By Category 5+, oxidation induced damage spreads to the top of the port walls. Category 6 burners show full fold fracture and consumption and substantial port opening in the hottest zones.

The burner fold failure process involves preferential oxide development at sites with manufacturing flaws. The level of temperature and the thermal cycling causes oxidation-induced consumption of the folds and the distortion to the port geometry.

The heat exchanger hot spot breakdown is the result of a similar oxidation-induced failure. The level of temperature along with the cycling of the furnace causes preferential oxidation, cracking, and spalling of the oxide, and further oxide growth.

CONCLUSIONS

The manufacturing process utilized by Consolidated for fabrication of the burner causes several flaws which are major contributors to the burner and heat exchanger failure process. The die stamped port openings have corners with insufficient corner radii. Upon folding and crimping, the inner corners crack. The fold forming radius is more acute than the minimum

recommended radius. As a result, the aluminum coating on the new, as-manufactured fold cracks, spalls, and loses adherence. The shear burr on each end of the fold splits and cracks during the folding process. Due to the manufacturing damage to the aluminum coating at the folds, the thermal rating of the burner metal decreases from a maximum of 1250°F for the aluminized material to 1000°F due to the now "exposed" low carbon steel base material.

During furnace operation, the NOx rods raise the temperatures to which the burners are exposed. With exposure to the NOx rod elevated temperatures, an oxidation-induced breakdown of the burner folds occurs. Preferential oxidation and crack propagation occurs at the shear burr cracks and the fold inner corner cracks. The folds eventually are consumed from excessive temperature and a thermal cycling-induced oxidation process.

Based on the color change on the sides of the burner tubes, it is clear that temperatures of 950°F are occurring several inches below the burner folds. This, along with spalling damages observed to the aluminum coating at the folds, supports the conclusion that the temperatures at the folds are at or above 1250°F. The as-manufactured folds are only capable of tolerating a maximum of 1000°F.

The NOx rod implementation on this burner causes temperatures to exceed that allowable for the materials. It must be noted that, to this date, no non-NOx rod burner has been examined which shows any burner fold cracking and/or degradation. Thus, the splitting and cracking that occurs during manufacturing is present on all burners, but the operating temperatures on units without NOx rods are insufficient to cause burner breakdown.

Once a sufficient number of burner folds have fully fractured/consumed, the thermal environment causes the burner ports to distort in an open mode. Eventually, a number of ports open

and combine into one large "port" which can include as many as 6 or more of the original ports. The resulting condition allows a large, "lazy" flame to exist. During the fold breakdown and into the port opening stages, the heat exchanger sustains a localized overheating which generates cracking and eventual rupture. The final stage in the heat exchanger failure process allows blower air to exit the exchanger rupture, impinging on the large lazy flame and forcing it downward and laterally. The flame can be forced out the side burner opening and ignite adjacent combustibles. During the same sequence, the flame and heat at the burners are blown downward into the panels below the burner. This increases the temperatures at the furnace to wood flooring interface, and leads to a pyrolytic decomposition.

Respectfully submitted,

Gerald F. Zamiski, Ph.D.
Professional Engineer
California No. MT1851

Paul S. Guthorn, M.S.M.E.
Professional Engineer
California No. M28649
California No. MT1845